第 48 卷 第 7 期
2021 年 7 月

湖南大学学报（自然科学版）
Journal of Hunan University（Natural Sciences）

Vol. 48. No. 7.
July 2021

Open Access Article

The Spatio-Temporal Variability of Chlorophyll-A and Its Physical Variables in the South Java Sea Shelf

Asep Sandra Budiman[1,2*], Dietriech Geoffrey Bengen[2], I. Wayan Nurjaya[2], Zainal Arifin[1], Muhammad Furqon Azis Ismail[1]

[1] Research Center for Oceanography, LIPI, Jakarta, Indonesia

[2] Faculty of Fisheries and Marine Sciences, IPB, Bogor, Indonesia

Abstract: The Chlorophyll-a (Chl-a) dynamics in the upwelling system associate with physical variables that accompany it, whether it is a driver or a response to the upwelling process. As an upwelling driver, wind and current could enhance the Chl-a concentration through a process known as wind-driven and current-driven upwelling, respectively. On the other hand, Sea Surface Temperature (SST) and Sea Surface Height Anomaly (SSHA) come as the upwelling response. We examine these four physical variables against the Chl-a dynamics in the South Java Sea shelf using satellite-derived and ocean reanalysis data from 2002 to 2017. Chl-a variability was examined using Empirical Orthogonal Function (EOF) to find spatial and temporal contrasting differences, then relate them to the physical variables. Our result exhibits seasonal patterns in the Chl-a variations, indicating the well-known South Java upwelling system, which is high during the south-east (SE) monsoon and low during the north-west (NW) monsoon. March and September were the two contrasting months shown by the significant differences of Chl-a, alongshore wind stress, SST, and SSHA between the two. The alongshore wind has a significant correlation with the Chl-a at the shelf area in September since wind-driven upwelling during that time. The alongshore bottom stress significantly correlates with the Chl-a at the 109.5˚E, 8˚S in March (wind-driven downwelling periods), indicating an upwelling-favorable current. However, the vertical cross-shelf temperature and alongshore current do not show a current-driven upwelling nor water masses uplift at this point in March.

Keywords: chlorophyll-a, physical variables, Empirical Orthogonal Analysis, South Java upwelling.

南爪哇海陆架叶绿素一种的时空变异性及其物理变量

摘要：上升流系统中的叶绿素-一种(叶绿素）动力学与伴随它的物理变量相关联，无论是驱动力还是对上升流过程的响应。作为上升流的驱动力，风和洋流可以分别通过称为风驱动和电流驱动的上升流的过程来提高叶绿素的浓度。另一方面，海面温度（不锈钢）和海面高度异常（SSHA）作为上升流响应。我们使用 2002 年至 2017 年的卫星衍生数据和海洋再分析数据，针对南爪哇海陆架的叶绿素动力学研究了这四个物理变量。使用经验正交函数(EOF）检查了叶绿素变异性，以找到空间和时间对比差异，然后将它们与物理变量联系起来。我们的结果展示了叶绿素变化的季节性模式，表明著名的南爪哇上升流系统在东南（东南）季风期间高，在西北（西北）季风期间低。 3 月和 9 月是两个截然不同的月份，两者之间的叶绿素、沿岸风应力、不锈钢和 SSHA 存在显着差异。 9 月陆架区沿风风与叶绿素具有显着相关性，因为当时风驱动上升流。沿岸底部应力与 3 月 109.5˚E、8˚S 的叶绿素显着相关（风驱动下流期），表明有利于上升流。然而，垂直跨大陆架温度和沿岸水流在 3 月的这个时间点没有显示出电流驱动的上升流或水团上升。

关键词：叶绿素-一种，物理变量，经验正交分析，南爪哇上升流。

Received: April 16, 2021 / Revised: May 17, 2021 / Accepted: June 14, 2021 / Published: July 31, 2021

About the authors: Asep Sandra Budiman, Research Center for Oceanography, LIPI, Jakarta, Indonesia; Faculty of Fisheries and Marine Sciences, IPB, Bogor, Indonesia; Dietriech Geoffrey Bengen, I. Wayan Nurjaya, Faculty of Fisheries and Marine Sciences, IPB, Bogor, Indonesia; Zainal Arifin, Muhammad Furqon Azis Ismail, Research Center for Oceanography, LIPI, Jakarta, Indonesia

Corresponding author Asep Sandra Budiman, assandra81@gmail.com

1. Introduction

As the major primary productivity producer in the ocean, phytoplankton is the base of marine food [1]–[3]. Chlorophyll-a (Chl-a) concentration has become widely used as the proxy of phytoplankton biomass [4]. The previous study has shown that Chl-a concentrations and the taxonomic composition of phytoplankton communities are qualitatively correlated with the physical variables [5], oceanic circulation, and mesoscale physical processes [6]–[8]. The Chl-a in the coastal upwelling system area has high variability as the upwelling, high during the upwelling period and mostly low during the non-upwelling or the downwelling period. The selective absorption of certain wavelengths (blue and blue-green) by Chl-a as a photosynthetic pigment allows the quantification of phytoplankton biomass through satellite-derived measurements of ocean color [9], [10].

Southern Java coast is well known as the upwelling system in the South East Tropical Indian Ocean (SETIO). Lies in the majority region of the ocean's productivity [11], the southern Java coast becomes the site of important fisheries in Indonesian waters [12], [13]. The oceanic and atmospheric process in this region may influence Chl-*a* concentrations, such as the monsoon system [14], tides [15], the Madden-Julian Oscillation (MJO) [14], [16], [17], Kelvin and Rossby waves [18], [19], the Indian Ocean Dipole (IOD) [20], the El-Niño Southern Oscillation (ENSO) [21], [41], the Indonesian Throughflow (ITF) [22], [23], the South Java Current (SJC) [22], [24], the South Equatorial Current (SEC) [22], and eddies [25], [26].

The southern Java upwelling responds to the monsoonal winds, which is associated with the seasonal southeasterly wind and well known as the wind-driven upwelling. In turn, southern Java waters rich in nutrients and Chl-a during the upwelling event. The study of [27] reveals a westward shift of upwelling signal along the southern Java coast, consistent with the alongshore wind shift.

Previous studies have shown that upwelling can be intensified or even be generated through both wind-driven and current-driven processes. In the case of current-driven processes, upwelling can be generated through 1) the interaction of boundary currents over variable topography [28]–[30], 2) encroachment of the boundary current flow to the coast [31], and 3) cyclonic eddies [25]. Current-driven upwelling is important since it has the same role as wind-driven upwelling in nutrient supply and biological productivity by increasing the Chl-a concentrations. According to the Java upwelling that occurs among the southern Sunda shelf area with several ocean circulations, i.e., the semi-annually reversing boundary current SJC and mesoscale eddies, the existences of current-driven upwelling or current-driven uplift would be possible along the southern coast of Java.

It is well documented that the isotherms are generally uplifted on the continental shelf adjacent to western boundary currents (WBCs) [32], [33] and have been shown to occur on the shelf adjacent to the East Australian Current (EAC) [31]. The evidence of the same process in the South Java shelf has not yet been found and would be a new finding. As the wind-driven upwelling system generates an Ekman layer at the surface, the current-driven upwelling generates a layer at the bottom depth, namely Bottom Boundary Layer (BBL) [34]. Onshore flow in the BBL can result as a response to interior flow along the continental shelf (poleward along an eastern coast in the Southern Hemisphere) or, in our case, westward flow along a southern Java coast. This onshore flow carries dense water up the slope like Ekman transport at the surface, resulting in upwelling.

We hypothesize that there is an uplift or upwelling process in the shelf area of South Java since it has met the requirements for the process to occur, i.e., the existence of oceanic circulations in the shelf and its adjacent areas such as boundary currents (South Java current) and eddies which could infringe the shelf break at a certain time and lift the water masses originating from the depth to the surface.

The previous study of South Java upwelling has focused more on studies during the south-east monsoon [21], [27], [35], while the conditions during the north-west monsoon are not widely known. [36] examine the condition of Indonesian waters during the NW monsoon but not focused on the South Java upwelling system. Here, for the first time, we reveal the physical condition of the South Java upwelling system during the north-west monsoon. The analysis is focused more closely on the shelf and the adjacent area because it has not been discussed before. We hypothesize that there is current-driven upwelling on the shelf.

Although South Java upwelling has been the focus of many researchers, studies of upwelling as part of the shelf circulation have not yet been conducted. For the first time, the Java upwelling (based on Chl-a concentration analysis) will be investigated closely in the shelf area by involving the various physical variables that accompanied the upwelling process. The alongshore bottom stress (hereafter referred to as bottom stress) as the agent to current upwelling or water masses uplift will be included and separately discussed. The bottom stress is expected to be directed mainly alongshore since alongshore flows generally predominate in the coastal ocean [37]. It has been

found that the bottom stress can be caused by the interaction between near-bottom currents by the boundary current, current encroachment, eddy activity, and rugged bathymetry [38]. The possibility of current-driven upwelling or water masses uplift due to upwelling-favorable bottom stress in the southern Java Sea shelf will be investigated for the first time. Enhanced Chl-a in this region is well known as a response to wind-driven upwelling. Still, the possibilities for other forces or processes (i.e., current-driven upwelling) that leading this phenomenon have never been studied and known well. In this study, we present the quantification of the contributions of the physical variables to Chl-a variability on the southern coast of Java. We aimed to: (1) describe the spatial and temporal distribution of Chl-a with a focus on the shelf region; (2) quantify the contribution made by four physical variables that accompanied the upwelling process as the main process influenced Chl-a variability in the South Java.

2. Materials and Method

2.1. General Features of the Study Area

The study site spanned longitudinally from 108˚E to 114˚E (Fig. 1), including the recently investigated upwelling region [9], [27], [39], [40]. The continental shelf (hereafter called shelf) presents different dimensions along the South Java coast. The Cilacapcoast shows the widest shelf (~125 km from the coast), followed by the Kretek coast (~75 km) and Prigicoast (~50 km). The eastern region has the narrowest shelf (~10 km) (Fig. 1).

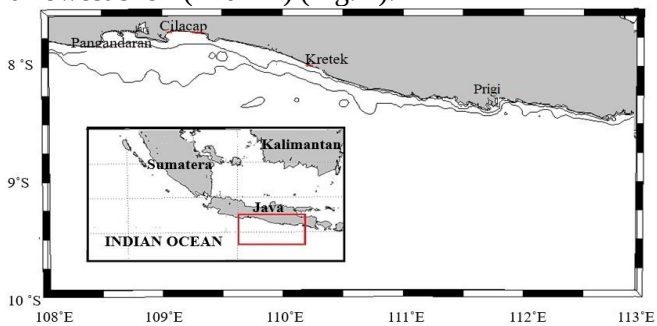

Fig. 1 The study area spanned at 108 – 114 º E, 7.5 – 10 ºS. Isobath 40 - 200 m is drawn by contour lines. Inset is our study domain among Indonesian islands

The circulation is influenced by the oceanic and atmospheric dynamics, which are seasonally reversing monsoonal wind [14], the intra-seasonally Kelvin waves during the transitional monsoon [18], [19], the Indian Ocean Dipole (IOD) [20], and ENSO [21], [41].

2.2. Surface Satellite Chlorophyll-a

Satellite remotely-sensed Chl-a (mg m^{-3}) data obtained from daily globally L4 ocean color reprocessed from [62]. The Chl-a data have a spatial resolution of about 4 km covering the period of 2002–2017. These Chl-a products (Daily, Monthly, and Climatology) are based on merging the sensors SeaWiFS, MODIS, MERIS, VIIRS-SNPP&JPSS1, OLCI-S3A&S3B. The application of remotely sensed Chl-a data is limited in shallow coastal shelf water due to a range of factors, including bottom albedo, suspended sediment, and coastal turbidity [42]. [43] restricting the interpretation and analysis to water deeper than 40 m. Here, the limitation of remotely sensed Chl-a concentrations was considered by taking the pixel of the Chl-a deeper than 40 m isobaths for further analysis.

2.3. Physical Variables

Physical variables promoted Chl-a variations in our domain considered both driver and response of South Java upwelling system. The driver was wind stress and bottom stress, while the response was Sea Surface Temperature (SST) and Sea Surface Height Anomaly (SSHA). A 10-m daily winds data used an ERA5, the fifth generation European Centre for Medium-Range Weather Forecasts (ECMWF) atmospheric reanalysis of the global climate for 2002–2017. The product has a 25 km spatial resolution and can be downloaded from [61]. Sea Surface Temperature (SST), Sea Surface Height (SSH), and bottom currents obtained from [61]. Sea Surface Temperature (SST), Sea Surface Height (SSH), and bottom currents obtained from GLOBAL_REANALYSIS_PHY_001_030 [44], distributed through the Copernicus Marine Environment Monitoring Service (CMEMS), a global ocean eddy-resolving (1/12° horizontal resolution, approximatively 8 km, and 50 vertical levels) reanalysis covering the altimetry era 1993-2018. It is based largely on the current real-time global forecasting CMEMS system. This product can be downloaded from [62]. The alongshore wind stress (hereafter referred to as wind stress) calculated by the following formulation

$$\tau_{wx} = \rho_a C_w u_w \sqrt{u_w^2 + v_w^2}$$

u_w (m s-1) and v_w (m s-1) are west-east and south-north wind velocity components. C_w is a velocity-dependent drag coefficient (0.0015)and $\rho_a$is the density of air with 1.3 kg m-3.Bottom stress (τ_{bx}) calculated using the current at the bottom level for 2002–2017. The formula to calculate τ_{bx} follows the theory applied by [43].

$$\tau_{bx} = \rho_w C_D u_b \sqrt{u_b^2 + v_b^2}$$

u_b (m.s^{-1}) and v_b (m.s^{-1}) are zonal and meridional components of bottom current velocity. C_d is a velocity-dependent drag (0.0025) coefficient and $\rho_w$is the density of seawater with 01025 kg m-3. The bottom current velocity component was not rotated to the alongshore direction, which potentially underestimated the bottom stress. τ_{wx} and τ_{bx} < 0 N m-2 was considered as upwelling favorable while τ_{wx} and τ_{bx}>

0 N.m-2 was considered as downwelling favorable.

2.4. Data Processing and Statistical Analysis

Chl-a and physical variables in the study region were analyzed through monthly mean climatology. The spatial and temporal variability of total Chl-a was determined using a standard Empirical Orthogonal Function (EOF) analysis with a singular value decomposition (SVD) technique. The method finds spatial patterns of variability, their time variation, and a measure of each pattern's magnitude [45]. EOF calculates a set of orthogonal functions or spatio-temporal components, which can be used for constructing the original data set at all points during the study periods. The first mode, having the largest eigenvalue, typically accounts for a considerable fraction of the variance of the data or explains the dominant variability of the data set. SVD is one of the primary methods for computing the EOFs for a grid of time series of observations besides the scatter matrix method [46]. Using the SVD method, we could quantify the total variance of the Chl-a concentration in both orthogonal and independent modes as it describes the temporal amplitudes of the spatial eigenvectors and their associated eigenvalues [47]. The result containing the highest percentage of the Chl-a variability, both spatial and temporal that allow us to determine (i) the most contrasting areas in terms of the spatial Chl-a variability and (ii) the main contrasting months in terms of the temporal Chl-a variability in the southern Java coast. This approach has been successfully determined the space-time features of Chl-a data [47].

For analyzing the physical variable's contribution and the prominent factors promoting the Chl-a variances, the Linear Pearson correlation analysis between Chl-a and the physical variables for the most contrasting month was performed by extracting the value of these variables at 10 points. The points were chosen in the domain according to the bathymetry and bottom stress features to cover the current-driven investigations on the shelf of our domain. For this, all the variables were re-gridded to the lowest spatial resolution (~25 km) as applied before [47]. Linear stepwise regression was performed at 10 points to assess the association between the Chl-a and its predicting physical variables for the most contrasting month. A stepwise method was chosen to find the best explanatory model from all the possible combinations of the predictor variables Akaike's information criterion (AIC) [48]. The smallest achieved value of AIC indicates the best model, i.e., the best combination of the physical predictor variables that explains the largest amount of the variation in the response variable (Chl-a).

The possibility of current-driven upwelling or water masses bottom uplift was investigated used vertical cross-shelf temperature and alongshore current. The section was made in the region with the most upwelling-favorable bottom stress features resulted from the Linear Pearson and stepwise regression models.

2.5. Data Reliability

2.5.1. Chlorophyll-a

The merged OC-CCI total Chl-a data product has several improvements, including inter-sensor bias-corrected time-series data that improves spatial and temporal coverage, maintains rigorous standards for data quality, error characterization, and per-pixel uncertainty characterization based on its validation [49].

2.5.2. Wind

The ECMWF-based wind has been used for inputs of many ocean models in marine forecasting, for ocean forces, including their associated biases [50]. ERA5 is the latest reanalysis dataset from the European Centre for Medium-range Weather Forecasts (ECMWF) after ERA-Interim [51]. ERA5 comes with many improvements compared with ERA-Interim, most notably better spatial (25 km) and temporal resolution (1h), a better representation of geophysical processes in the forecast model, and more extensive observational inputs to the data assimilation system [52]. Besides, it is archived at the hourly time step, uses a more advanced assimilation system, and includes more sources of data [53]. It is produced using high-resolution forecasts (HRES) at 25 km resolution (one-fourth of the spatial resolution of the operational model), and it computes atmospheric variables at 139 pressure levels. Data for the 1979–2018 period were released in March 2019, and in the next few years, the dataset will cover the period from 1950 to near real-time [54]. Atmospheric data on these levels are interpolated to 37 pressure levels (the same levels as in ERA-Interim). Many researchers have widely used the dataset and can conduct comprehensive global simulations, long-term simulations for climate studies [52]. ERA5 winds show a 20% improvement relative to ERA-Interim and perform better in terms of mean and transient wind errors, wind divergence, and wind stress curl biases [50].

2.5.3. Reanalysis Data

Reanalysis data has been widely used in atmospheric sciences to assess the impact of observing system changes, gauge progress in modeling and assimilation capabilities, and obtain state-of-the-art climatologies to evaluate forecast-error anomalies [51]. The product GLOBAL-REANALYSIS-PHY-001-030 (hereafter called GLORYS12V1 reanalysis) consists of global ocean reanalyses datasets at 1/12° horizontal resolution. [55] obtained a series of diagnostics on

GLORYS12V1 reanalysis with several summaries, which will be described in this section. In terms of SST data, the reanalysis is very stable from the 2000's up to 2016. The global mean SST of GLORYS12V1 reanalysis is close to the observations with a weak (warm) misfit of less than 0.1°C all along with the reanalysis. The global positive SST linear trend is highly consistent with AVHRR data. Since a small warm bias (up to 0.1°C) was found in the 0-500 m layer (located between 100 and 200 m), the reanalysis beat the climatology for the bias and the RMS with lower RMS differences in the 0-500 m layer depth. In terms of ocean current, this reproduces well the main ocean currents. Root Mean Square Difference (RMSD) is generally smaller than 0.25 $m.s^{-1}$ in the water column. In terms of SSHA, GLORYS12V1 reanalysis is very close to altimetric observations and has a good ability to describe the sea level variability. Regional trends are particularly well reproduced. Unfortunately, however, the globally averaged sea level trend is slightly underestimated (2.66 mm $year^{-1}$) compared to the Aviso SLA CCI observed estimates (3.27 mm $year^{-1}$). A global and constant 0.07 cm bias is present during the 2005-2016 time period. However, long-term in-situ observations data are highly suggested to get more ample evidence for supporting our result.

3. Results

3.1. Spatio-Temporal Variability of the Annual Cycle of Chlorophyll-a

The annual climatological cycle of Chl-a shows a seasonal pattern in the oceanic region, with the highest Chl-a concentration values from June to November (> ~1.5 mg m^{-3}) and the lowest, from December to May (< ~1 mg m^{-3}; Fig. 2).

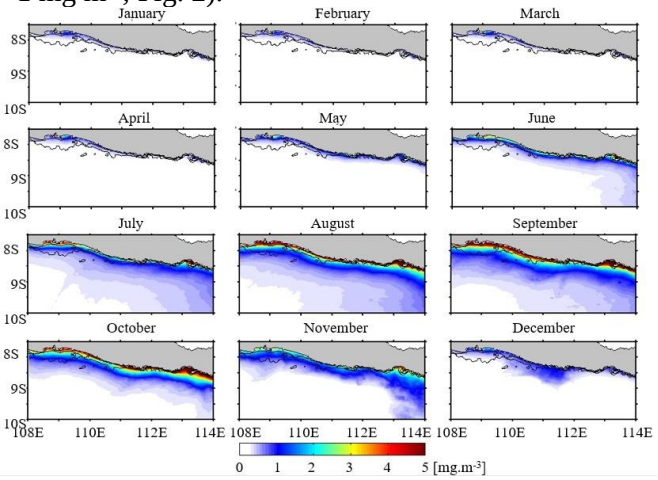

Fig. 2 Monthly mean climatology of total chlorophyll-a (Chl-a) in the southern Java coast from January 2002 to December 2017. The Chl-a is represented by a color scale

The shelf region has the highest Chl-a throughout a year with a value above the background (0.2 mg m-3). The high Chl-a seems to propagate westward from June and reach its peak during September, while Chl-a with value > ~0.25 mg m-3 was covered more than half of our study domain. This propagation encountered relaxation during October and November. The relaxation remains Chl-a with a value of 0.25 – 1 mg m^{-3} across the shelf during December. Chl-a with value > ~2 mg m-3 formed a band of high value in the shelf during August and becomes wider during September and October until crossing the shelf mostly in the eastern region.

The Empirical Orthogonal Functions (EOFs) from the monthly total Chl-a values revealed a seasonal signal shown by the first and second modes, explaining 95.88% of the total variance in the annual cycle of Chl-a in the domain (Fig. 3). The first mode explains 92.12% of the Chl-a annual variability, while the second mode explains 3,76% (Fig. 3A, B). The temporal EOF of the first mode (Fig. 3A) showed a noted seasonal pattern, characterized by increasing Chl-a from August to October, coincident with the high amplitude of the annual cycle (> ~0.01) along the southern Java sea shelf in our domain decreasing towards the oceanic zone (Fig. 3C). The second mode showed a smaller amplitude in both spatial and temporal modes than Mode 1 (Fig. 3B, D). According to this result, in terms of the temporal variability, March and September were chosen as the most contrasting months for further analysis to explain the Chl-a variation connected with the physical drivers. In terms of the spatial variability of Chl-a, we expected different behavior in the shelf regions according to the marked amplitude resulted from spatial EOF modes and the bathymetry features; the one is in the western side, that is the region between 108.5˚E – 109.5˚E, and the other is in the region between 112˚E – 113˚E, the narrow shelf.

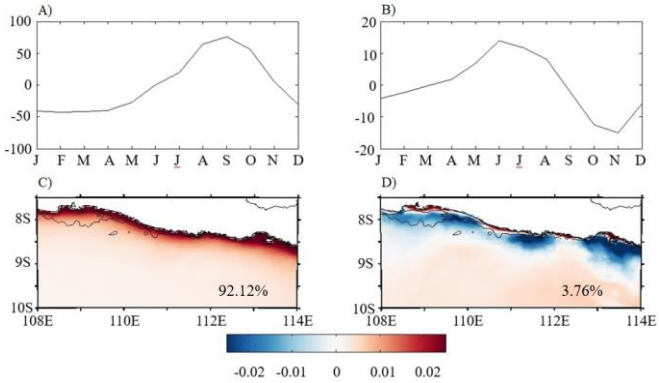

Fig. 3 Two modes of Principal Empirical Orthogonal Function (EOF) resulted from the annual climatological cycle of the total Chl-a in the South Java region: A, B - temporal EOF modes, C, D - corresponding spatial EOF modes

3.2. Spatial Patterns of the Physical Variables in March and September

3.2.1. Wind Stress and Bottom Stress

In March, the wind stress was downwelling favorable ($\boldsymbol{\tau_{wx} > 0}$), which covered the whole oceanic region of our domain (Fig. 4A). The western side of the

oceanic region, particularly the area between 8-9˚S and 108-109˚E, encounters the highest wind stress (>0.2 N m^{-2}), decreasing towards the eastern side of the domain and shelf. Compare with March, the wind stress in September was higher but in reverse directions. During this time, wind stresses mostly upwelling favorable ($\boldsymbol{\tau_{wx} < 0}$) with the lowest value (<0.02 N m^{-2}) at the eastern and the shelf increasing towards the western side off the coast (Fig. 4B).

Monthly climatology of the bottom stress revealed a marked region with westward circulations or upwelling favorable bottom stress ($\boldsymbol{\tau_{bx} < 0}$) in the shelf area, varies from 0.02 to 0.1 N m^{-2}, spanning longitudinally from 108.5˚E until 112.5˚E in March but not in September (Fig. 4C). According to the contrasting conditions, this area will be chosen for further examination to understand better the connection between Chl-a dynamics and its physical driver. Another notable feature is the weak westward circulation (-0.03 N $m^{-2} < \boldsymbol{\tau_{bx}} <$ -0.01 N m^{-2}) off the coast at the position of 9.5˚S, 110˚E and 9.5˚S, 111˚E (Fig. 4, top). In September, the bottom stress mostly downwelling favorable ($\boldsymbol{\tau_{bx} > 0}$) with the highest value in the shelf area (0.05 – 0.1 N m^{-2}) decreasing towards off coast.

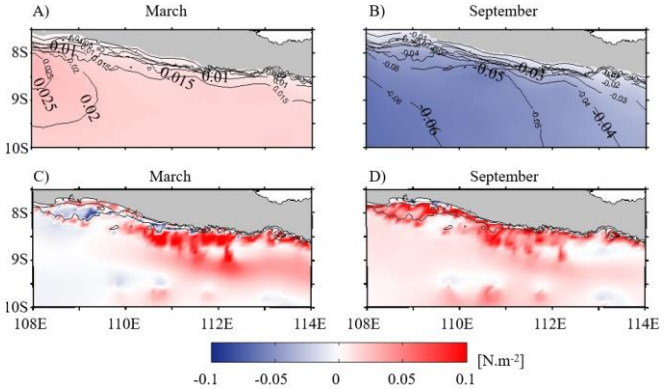

Fig. 4 Monthly climatology (2002–2016) of wind stress (A, B) and bottom stress (C, D) for March (A, C) and September (B, D). Blue (Red) shading represents the regions of upwelling (downwelling) favorable

3.2.2. Sea Surface Temperature (SST) and Sea Surface Height Anomaly (SSHA)

In March, SST varies from 29.2 to 29.5˚C with SSHA higher (> 0.05 m) along the coast and at the center off coast of the domain than in the western part of the domain (< 0.04 m) (Fig. 5A, B). In September, the surface temperature was colder than in September with a value lower near the coast (<25 ˚C) increasing towards off coast to value >26 ˚C with SSHA lower along the shelf and in the eastern part of the domain (< -0.16 m) gradiently decreased towards southwestern corner of the domain (Fig. 5C, D, bottom).

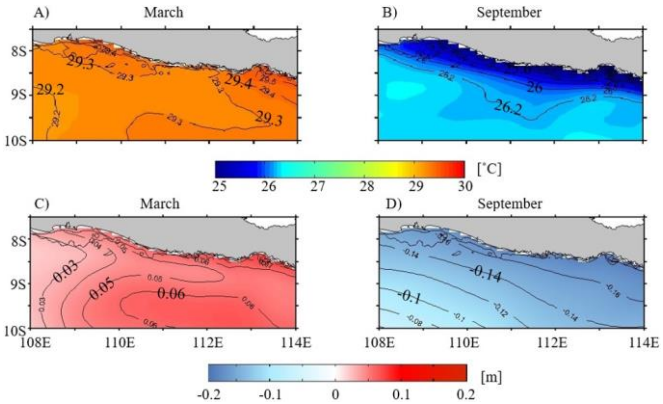

Fig. 5 Monthly climatology (2002–2017) of Sea Surface Temperature (SST) (A, B) and Sea Surface Height anomaly (SSHA) (C, D) for March and September. Red (blue) shading in the SST and SSHA plot represents the regions with warm (cold) and the regions with sea level anomalies above (below) the regional average, respectively. The value is plotted by a contour line

3.2.3. Pearson Analysis and Stepwise Regression Model

The Pearson analysis and stepwise regression model were performed at 10 points at the shelf break (depth ± 200 m) and adjacent area by considering the spatially bottom stress features and data availability to understand better the connection between Chl-a and the physical variables (Fig. 7).

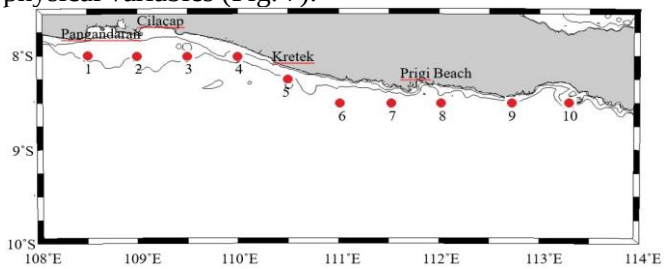

Fig. 7 10 longitudinally points where Pearson correlation analysis was performed. Points were chosen according to their bathymetry and bottom stress features. In terms of bottom stress features, Points 1-3 represent the area with upwelling-favorable, while Points 6-8 represent the area with strong downwelling-favorable bottom stress in March (Fig. 4B)

Pearson analysis from the monthly climatology data shows no correlation between Chl-a and SSHA in March. Several points showed the correlation between Chl-a and SST at the western points (Points 2-4) and the easternmost point (Point 10) with a 0.05 significance level. Still, in March, Chl-a correlated with the wind stress at Point 5 and correlated with the bottom stress at Point 3 at the 0.05 significance level. It can be concluded that the physical variables have a weak correlation to Chl-a variance at most of the points in March. In September, Chl-a has a significant correlation with SST, SSHA, and wind stress at most of our analysis points. In September, The SST and SSH at the western part (Points 1-5) and the eastern part (Points 8-10) have a significant correlation at the 0.05 level with Chl-a. Only two physical variables showed a significant correlation with Chl-a at the 0.01 level, SST at Point 9 and SSHA at Point 4. The alongshore wind

mostly correlated with Chl-a at the western part (Points 1-5) and the easternmost points (Point 10) with only the alongshore bottom stress at Point 2, which significantly correlated with Chl-a at the 0.05 level.

Table 1 Pearson correlation analysis results from monthly mean Chla and physical variables at each point during two contrasting months. Only values with significance at the 0.01 (**) and 0.05 (*) levels were shown

Mar	**Points**									
	1	**2**	**3**	**4**	**5**	**6**	**7**	**8**	**9**	**10**
SST	-	-0.51*	-0.54*	-0.62*	-	-	-	-	-	-0.64*
SSHA	-	-	-	-	-	-	-	-	-	-
τ_{wx}	-	-	-	-	0.57*	-	-	-	-	-
T_{bx}	-	-	0.58*	-	-	-	-	-	-	-
Sep	**Points**									
	1	**2**	**3**	**4**	**5**	**6**	**7**	**8**	**9**	**10**
SST	-0.58*	-0.57*	-0.59*	-0.64*	-0.52*	-	-	-0.55*	-0.65**	-0.62*
SSHA	-0.59*	-0.58*	-0.59*	-0.66**	-0.60*	-	-	-0.55*	-0.62*	-0.59*
τ_{wx}	0.62*	0.62*	0.54*	0.58*	-	-	-	-	-	0.57*
T_{bx}	-	0.62*	-	-	-	-	-	-	-	-

Note: Mar: March; Sep: September; SST: Sea Surface Temperature; SSHA: Sea Surface Height Anomaly; τ_{wx} and τ_{bx}: wind stress and bottom stress, respectively

In March, the stepwise regression model is relatively poor to model the combination of physical variables and its interaction in explaining the Chl-a dynamics (R^2<0.5), even though the model was significant in describing the observation (p-model < 0.05) at several points (Table 2). The results noted that τ_{bx} was significant in explaining the Chl-a dynamics at Point 3 (p-value = 0.05), while SST and τ_{bx} were significant at Point 10 (p-value =5.3e-04 and 0.007 respectively). In September, the wind usually occurs as a predictor of Chl-a functions at all points with a significant p-value, particularly at the westernmost and easternmost points (Points 1–5 and 9-10, respectively). For this result, it can be concluded that wind is the main force to the Chl-a dynamic in September. Besides the partitional contributions, several interaction terms were shown as a predictor in the regression models, significantly at the westernmost Points 1-4 in September (Table 2).

Table 2 The stepwise linear regression to obtain the physical variables and their interaction in explaining the Chlorophyll-a dynamics in the South Java Sea shelf for March (MAR) and September (SEP). The conditional tests show the best combination of the Physical predictor variables used in this study that explain the largest amount of the variation in the response variable (Chl-a) based on the smallest value of Akaike's information criterion (AIC). R^2 is the proportion of the explained variation for the model, p-model is the p-value of the model to show how significant the model to the observation is. The sign ":" between two variables in the predictor (p-value) columns indicates interaction between the two. Only significant values are shown ($p < 0.05$)

	Points	**R^2**	**p-model**	**AIC**	**Predictors (p-value)**
	1	0.24	-	-39.33	SSHA(-)
	2	0.49	0.05	-42.56	SST(-),τ_{bx}(-), SST: τ_{bx}(-)
	3	0.49	0.02	-40.42	SST(-),τ_{bx}(0.05)
	4	0.39	0.01	-30.52	SST(0.01)
MAR	5	0.44	0.03	-21.98	SST(-),τ_{wx}(-)
	6	0.14	-	-55.92	SSHA(-)
	7	0.20	-	-43.69	τ_{wx}(-)
	8	0.23	-	-42.95	τ_{wx} (-)
	9	0.26	0.05	-29.88	SST(0.05)
	10	0.68	0.001	-54.32	SST(5.3e-04), τ_{wx}(0.007)
	Points	**R2**	**p-model**	**AIC**	**Predictors (p-value)**
	1	0.88	2.1e-05	35.34	SSHA(0.0001), τ_{wx}(0.00007),SSHA: τ_{wx}(0.005)
	2	0.92	1.6e-05	35.77	SSHA(0.01), τ_{wx}(0.00007), τ_{bx}(0.006), τ_{wx}: τ_{bx}(0.01)
	3	0.85	6.7e-05	41.90	SST(0.0002), τ_{wx}(0.0004),SST: τ_{wx}(0.003)
	4	0.86	0.0002	65.17	SST(-),SSHA(0.04), τ_{wx}(0.0007),SSHA: τ_{wx}(0.01)

SEP	5	0.77	8e-04	61.72	SSHA(0.0005), τ_{wx}(0.002),SSHA: τ_{wx}(-)
	6	0.32	-	62.57	SSHA(-),τ_{wx}(-)
	7	0.34	-	56.28	SSHA(-),τ_{wx}(-)
	8	0.30	0.03	38.03	SSHA(0.03)
	9	0.26	0.05	-29.88	SST(0.002), τ_{wx}(0.02),SST: τ_{wx}(0.006)
	10	0.68	0.001	-54.32	SST(0.03), τ_{wx}(0.05),SST: τ_{wx}(0.06)

Note: The predictors are SST: Sea Surface Temperature, SSHA: Sea Surface Height Anomaly, τ_{wx} and τ_{bx}: wind stress and bottom stress, respectively

3.2.4. Cross-Shelf Temperature and Alongshore Current Vertical Section

According to the result described above, Pearson analysis and regression model noted that the bottom stress usually occurred as a variable that influenced the Chl-a dynamics at Point 3 with a significant correlation value. This result leads to the further investigation of the current-driven upwelling occurrences at Point 3. The vertical section of the monthly mean temperature and the alongshore current was performed to assess the bottom uplift caused by the encroaching boundary current at the shelf edge.

The vertical section of the monthly mean cross-shelf alongshore current (in this case: zonal current) and temperature at 119.5˚E, from 7.8 – 8.2 ˚S shows the process that occurred in the water column in March 2013 compare to September 2013 (Fig. 8). The year 2013 was chosen since it is the normal year of upwelling (a year with no positive IOD nor ENSO, Fig. 8 in [27]) to see the differences of the water column condition between two contrasting months in the same year. In March 2013, the alongshore current mostly flowed westward (U_0<0) at the depth above 200 m, including at Point 3, and encroached the shelf edge (Fig. 8A). In terms of bottom stress, it's upwelling-favorable bottom stress. Coinciding with these conditions, the isotherm, particularly 15-25 ˚C, is mostly deeper at the shelf edge than offshore or with no uplift at the shelf edge (Fig. 8A). An eastward flow dominantly occurs offshore at a depth below 300 m (Fig. 8A). Contrastly, in September 2013, the current mostly flows eastward (U_0>0) at a depth above 200 m, including at Point 3 with a small part of a westward flow at depth below 300 m offshore (Fig. 8B). The isotherm bands of 20 ˚C were found at the shallower depth in this month (<200 m) than in March (>200 m) since September is a wind-driven upwelling period. Besides, isotherm 25 ˚C, which was found at a depth below 100 m in March, reaches the near-surface depth (±25 m) in this month (Fig. 8B). The same process (a westward flow in March and an eastward flow in September) occurs every year at this point with different patterns and strengths due to additional forces differences each year, such as the existence of positive IOD or ENSO.

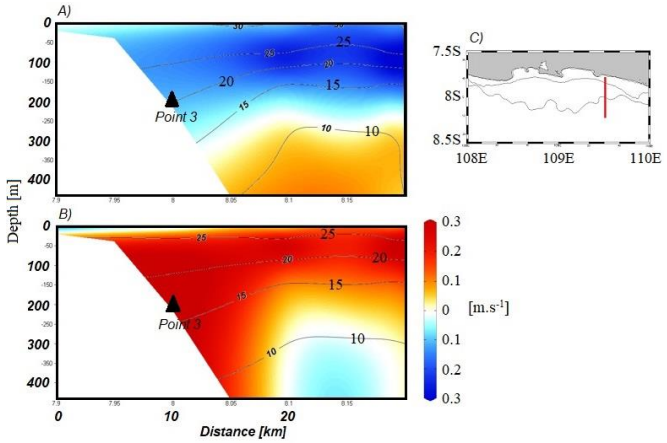

Fig. 8 Vertical section of the monthly mean cross-shelf current velocity snapshot (shading) with temperature contours (black lines) at 109.5E, from 7.8S to 8.2S (*C*) on (*A*) March 2013 and (*B*) September 2013. Black triangles show Point 3 location among the section. Red shading/ Positive value (blue shading /negative value) represents the eastward (westward) flow. Bottom shelf use bathymetry from ETOPO1.Isobath 40 and 200 m marked by contour lines in (*C*)

4. Discussion

Monthly mean climatology revealed Chl-a patterns seasonally with a high value (>0.2 mg m^{-3}) during SE monsoon (May - September) while the upwelling occurs in this region but not during NW monsoon as reported earlier by [36], [56]. Chl-a started to increase in May and peaked in September. The upwelling signal represented by high Chl-a, as seen in Fig. 2, was moved westward [27]. The seasonal signal of Chl-a was strongly explained by the first mode of EOF analysis result, which explains 95.88% of the total variance in the annual cycle of Chl-a. The temporal EOF of the first mode showed March and September as the months of lowest and highest Chl-a, respectively, which were considered two contrasting months for further analysis.

March is the period of downwelling favorable wind, which represents positive wind stress as the westerly NW monsoonal winds blow during this time. The condition reverses during September while the wind stress was upwelling favorable ($\tau_{wx} < 0$) as the southeasterly SE monsoonal wind blows in our domain during this time. This result was relevant to the earlier study of South Java upwelling, which is associated with the seasonal southeasterly wind.

According to the bottom stress patterns, the circulation at the shelf edge could be associated mainly with the semi-annually boundary current SJC, relevant with the pattern found by [57] that at the beginning of

the mooring in mid-March 1997, the daily averaged surface current at 55 and 115 are toward the north-west (Fig. 2B and 2C in [57]) and remains to the south-east at all depths from August until October. Further studies are still needed to obtain the contribution of the individual process to the net flow for detailed results.

According to the Pearson analysis, September has many more physical variables correlated with Chl-a than March due to upwelling during this time. During the upwelling period (SE monsoon), the alongshore wind drives the water masses' movements at the surface offshore, causing the low SSHA near the coast, and generates vertical motion of cold water masses from the depth to the surface, decreasing the SST. The ocean upwelling associated with this ocean-atmosphere feedback process was studied by [58]. It can be seen that Chl-a significantly correlated at 0.05 significance level with SST, SSHA, and wind stress at most of the points located at the shelf (Table 1). The wind stress usually occurs as a predictor with a significant value in the stepwise linear regression at most of the western and easternmost points (Table 2). We suggested that winds are the main driver of Chl-a dynamics through wind-driven upwelling at the shelf area during September or the upwelling period. This result relevant to previous studies of South Java upwelling [35].

Contrastly, Chl-a at Points 6 and 7 were not shown any significant correlation with the physical variables, both in March and September. We conclude that the physical variables used in this study highly influenced the Chl-a in the shelf area. Even though most of the physical variables have not shown a significant correlation with the Chl-a in March, the Pearson analysis reveals an important result that the bottom stress was significantly correlated with Chl-a at Point 3, where it was an upwelling-favorable bottom stress (negative bottom stress) region as shown in Fig. 4B. Besides, the stepwise linear regression reveals the important role of the bottom stress at Point 3 since it is a significant predictor in the model. These results lead the further investigation to reveal the possibilities of current-driven upwelling occurrence or water masses uplift at this point.

The vertical section of the cross-shelf temperature gradient (Fig. 8A) does not show the current-driven upwelling nor the water masses uplift, although there was an upwelling favorable bottom stress due to encroaching westward bottom flow at the shelf edge. We suggested that the upwelling-favorable bottom stress at Point 3 in March is insufficient to lift dense water or nutrient-rich water through onshore flow in the BBL to the shallower depth. In turn, it couldn't enhance the Chl-a at the surface. This conclusion can be seen in Fig. 2 that Chl-a is relatively lower in March (<1 mg m^{-3}) than in September (>1.5 mg m^{-3}) at the shelf. This result further confirms that upwelling in the southern coast of Java only occurs in the SE monsoon (June-September) but does not occur in the NW monsoon (December-March).

This study uses remotely-sensed and reanalysis data; no in-situ data is used. Future studies are encouraged, combining in situ experiments with satellite-based measurements and reanalysis data for better analysis and results. The Chl-a variability only involves four upwelling variables SST, SSHA, wind stress, and bottom stress. Other influencing factors to phytoplankton growth and its Chl-a biomass, such as light availability and nutrients [47], [59], are not involved and need to be considered in interpreting the results. In addition, Chl-a, which represents phytoplankton communities and biomass, are governed by many limiting and controlling factors, such as nutrient availability, light climate, temperature, salinity, competition, parasites, and grazing [60]. Even though the analysis presented here focuses largely on the monthly climatology, the data used here have a relatively long time series (almost two decades). They have provided sufficient results relevant to previous research.

5. Conclusions

Chl-a was varied seasonally in our domain with a higher value during SE monsoon than NW monsoon due to upwelling. The alongshore winds were the major variable influencing the Chl-a dynamic in the shelf area during the upwelling period. During the downwelling period, bottom stress significantly correlates with the Chl-a at the 109.5E, 8S of our domain. There was upwelling-favorable bottom stress at Point 3 in March, but the vertical section of the cross-shelf temperature gradient does not show the current-driven upwelling nor the water masses' uplift. In turn, it couldn't enhance the Chl-a at the surface. The physical variables used in this study (SST, SSHA, wind stress, and bottom stress) significantly correlate with Chl-a in the shelf area. They highly suggest that the southern Java upwelling studies cannot ignore the shelf process. Future studies are encouraged, comparing the process and conditions in the shelf area and its open waters.

Finally, it is highly suggested to combine different observational (in situ and satellite data) and modeling tools to evaluate our studies, particularly in the same domain or points. We expect that this study will supply additional information in understanding the productive dynamics of the South Java coast, leading to better management decisions regarding fisheries, tourism centers, and environmental policies.

Acknowledgment

The study was fully funded by LIPI's COREMAP CTI 2021 2022 (17/A/DK/2021). ASB acknowledges Lembaga Ilmu Pengetahuan Indonesia (LIPI) for supporting this study through the Doctoral By-Research Programs. We acknowledge the E.U.

Copernicus Marine Service Information that provided satellite data. The manuscript is part of doctoral theses in the Faculty of Fisheries and Marine Sciences, Institut Pertanian Bogor (IPB), Bogor, Indonesia.

References

[1] ROSS T., CRAIG S. E., COMEAU A., DAVIS R., DEVER M., and BECK M. Blooms and subsurface phytoplankton layers on the Scotian Shelf: Insights from profiling gliders. *Journal of Marine Systems*, 2017, 172: 118–127. https://doi.org/10.1016/j.jmarsys.2017.03.007

[2] TWEDDLE J. F., GUBBINS M., and SCOTT B. E. Should phytoplankton be a key consideration for marine management? *Marine Policy*, 2018, 97: 1–9. https://doi.org/10.1016/j.marpol.2018.08.026

[3] ARMENGOL L., CALBET A., FRANCHY G., RODRÍGUEZ-SANTOS A., and HERNÁNDEZ-LEÓN S. Planktonic food web structure and trophic transfer efficiency along a productivity gradient in the tropical and subtropical Atlantic Ocean. *Scientific Reports*, 2019, 9: 2044. https://doi.org/10.1038/s41598-019-38507-9

[4] SALGADO-HERNANZ P. M., RACAULT M. F., FONT-MUÑOZ J. S., and BASTERRETXEA G. Trends in phytoplankton phenology in the Mediterranean Sea based on ocean-colour remote sensing. *Remote Sensing of Environment*, 2019, 221: 50–64. https://doi.org/10.1016/j.rse.2018.10.036

[5] LIM Y. K., BAEK S. H., LEE M., KIM Y. O., CHOI K. H., and KIM J. H. Phytoplankton composition associated with physical and chemical variables during summer in the southern sea of Korea: Implication of the succession of the two toxic dinoflagellates Cochlodinium (a.k.a. Margalefidinium) polykrikoides and Alexandrium affine. *Journal of Experimental Marine Biology and Ecology*, 2019, 516: 51–66. https://doi.org/10.1016/j.jembe.2019.05.006

[6] CORREDOR-ACOSTA A., MORALES C. E., BREWIN R. J. W., AUGER P.-A., PIZARRO O., HORMAZABAL S., and ANABALÓN V. Phytoplankton size structure in association with mesoscale Eddies off Central-Southern Chile: The satellite application of a phytoplankton size-class model. *Remote Sensing*, 2018, 10(6): 834. https://doi.org/10.3390/rs10060834

[7] RUIZ S., CLARET M., PASCUAL A., OLITA A., TROUPIN C., CAPET A., TOVAR-SÁNCHEZ A., ALLEN J., POULAIN P.-M., TINTORÉ J., and MAHADEVAN A. Effects of Oceanic Mesoscale and Submesoscale Frontal Processes on the Vertical Transport of Phytoplankton. *Journal of Geophysical Research: Oceans*, 2019, 124(8): 5999–6014. https://doi.org/10.1029/2019JC015034

[8] GEBREHIWOT M., KIFLE D., and TRIEST L. Partitioning the influence of hydrodynamics-induced physical variables and nutrients on phytoplankton assemblages in a shallow tropical reservoir (Koka, Ethiopia). *Limnology*, 2020, 21(3): 269–274. https://doi.org/10.1007/s10201-020-00611-5

[9] GAO C., FU M., SONG H., WANG L., WEI Q., SUN P., LIU L., and ZHANG X. Phytoplankton pigment pattern in the subsurface chlorophyll maximum in the South Java coastal upwelling system, Indonesia. *Acta Oceanologica Sinica*, 2018, 37(12): 97–106. https://doi.org/10.1007/s13131-018-1342-x

[10] GROOM S. B., SATHYENDRANATH S., BAN Y., BERNARD S., BREWIN R., BROTAS V., BROCKMANN C., CHAUHAN P., CHOI J.-K., CHUPRIN A., CIAVATTA S., CIPOLLINI P., DONLON C., FRANZ B., HE X., HIRATA T., JACKSON T., KAMPEL M., KRASEMANN H., LAVENDER S., PARDO-MARTINEZ S., MÉLIN F., PLATT T., SANTOLERI R., SKAKALA J., SCHAEFFER B., SMITH M., STEINMETZ F., VALENTE A., and WANG M. Satellite ocean colour: Current status and future perspective. *Frontiers in Marine Science*, 2019, 6: 485. https://doi.org/10.3389/fmars.2019.00485

[11] HOOD R. R., BECKLEY L. E., and WIGGERT J. D. Biogeochemical and ecological impacts of boundary currents in the Indian Ocean. *Progress in Oceanography*, 2017, 156: 290–325. https://doi.org/10.1016/j.pocean.2017.04.011

[12] LAHLALI H., WIRASATRIYA A., GENSAC E., HELMI M., KUNARSO, and KISMAWARDHANI R. A. Environmental aspects of tuna catches in the Indian Ocean, southern coast of Java, based on satellite measurements. Proceedings of the 4th International Symposium on Geoinformatics, Malang, 2018, pp. 1-6. https://doi.org/10.1109/ISYG.2018.8612020

[13] DEWI A. K., GAOL J. L., SIREGAR V. P., and ATMADIPOERA A. S. Bigeye tuna fishing ground analysis using oceanographic features in Eastern Indian Ocean off Southern Java. *IOP Conference Series: Earth and Environmental Science*, 2020, 429: 012043. https://doi.org/10.1088/1755-1315/429/1/012043

[14] DUAN Y., LIU H., YU W., LIU L., YANG G., and LIU B. The onset of the Indonesian–Australian summer monsoon triggered by the first-branch eastward-propagating Madden–Julian oscillation. *Journal of Climate*, 2019, 32(17): 5453–5470. https://doi.org/10.1175/JCLI-D-18-0513.1

[15] RUDIASTUTI A. W., SYAFI'I A. N., and KUSUMA H. A. Spatial pattern of tides in Indonesia using altimetry data. Proceedings of the 6th International Symposium on LAPAN-IPB Satellite, Bogor, 2019. https://doi.org/10.1117/12.2542855

[16] KIM H., VITART F., and WALISER D. E. Prediction of the Madden-Julian oscillation: A review. *Journal of Climate*, 2018, 31(23): 9425–9443. https://doi.org/10.1175/JCLI-D-18-0210.1

[17] ZHANG C., ADAMES F., KHOUIDER B., WANG B., and YANG D. Four Theories of the Madden-Julian Oscillation. *Reviews of Geophysics*, 2020, 58(3): e2019RG000685. https://doi.org/10.1029/2019RG000685

[18] MENEZES V. V., & VIANNA M. L. Quasi-biennial Rossby and Kelvin waves in the South Indian Ocean: Tropical and subtropical modes and the Indian Ocean Dipole. *Deep Sea Research Part II: Topical Studies in Oceanography*, 2019, 166: 43–63. https://doi.org/10.1016/j.dsr2.2019.05.002

[19] PUJIANA K., & MCPHADEN M. J. Intraseasonal Kelvin Waves in the Equatorial Indian Ocean and Their Propagation into the Indonesian Seas. *Journal of Geophysical Research: Oceans*, 2020, 125(5): 1–25. https://doi.org/10.1029/2019JC015839

[20] HAMEED S. N. The Indian Ocean Dipole. *Oxford Research Encyclopedias: Climate Science*, 2018, 1: 1–35. https://doi.org/10.1093/acrefore/9780190228620.013.619

[21] WIRASATRIYA A., KUNARSO K., MASLUKAH L., SATRIADI A., and ARMANTO R. D. Different responses of chlorophyll-a concentration and Sea Surface Temperature (SST) on southeasterly wind blowing in the Sunda Strait.

IOP Conference Series: Earth and Environmental Science, 2018, 139: 012028. https://doi.org/10.1088/1755-1315/139/1/012028
[22] NINGSIH N. S., SAKINA S. L., SUSANTO R. D., and HANIFAH F. Zonal Current Characteristics in the Southeastern Tropical Indian Ocean (SETIO). *Ocean Science Discussions*, 2020. https://doi.org/10.5194/os-2020-91
[23] PANG X., BASSINOT F., and SEPULCRE S. Indonesian Throughflow variability over the last two glacial-interglacial cycles: Evidence from the eastern Indian Ocean. *Quaternary Science Reviews*, 2021, 256: 106839. https://doi.org/10.1016/j.quascirev.2021.106839
[24] UTARI P. A., SETIABUDIDAYA D., KHAKIM M. Y. N., and ISKANDAR I. Dynamics of the South Java Coastal Current revealed by RAMA observing network. *Terrestrial, Atmospheric and Oceanic Sciences*, 2019, 30(2): 235–245. https://doi.org/10.3319/TAO.2018.12.14.01
[25] YANG G., ZHAO X., LI Y., LIU L., WANG F., and YU W. Chlorophyll variability induced by mesoscale eddies in the southeastern tropical Indian Ocean. *Journal of Marine Systems*, 2018, 199: 103209. https://doi.org/10.1016/j.jmarsys.2019.103209
[26] ISMAIL M. F. A., RIBBE J., ARIFIN T., TAOFIQUROHMAN A., and ANGGORO D. A census of eddies in the tropical eastern boundary of the Indian Ocean. *Journal of Geophysical Research: Oceans*, 2021, 126(6): e2021JC017204. https://doi.org/10.1029/2021JC017204
[27] WIRASATRIYA A., SETIAWAN J. D., SUGIANTO D. N., ROSYADI I. A., HARYADI H., WINARSO G., SETIAWAN R. Y., and SUSANTO R. D. Ekman dynamics variability along the southern coast of Java revealed by satellite data. *International Journal of Remote Sensing*, 2020, 41(21): 8475–8496. https://doi.org/10.1080/01431161.2020.1797215
[28] DAI S., ZHAO Y., LI X., WANG Z., ZHU M., LIANG J., LIU H., TIAN Z., and SUN X. The seamount effect on phytoplankton in the tropical western Pacific. *Marine Environmental Research*, 2020, 162: 105094. https://doi.org/10.1016/j.marenvres.2020.105094
[29] JUNG G., & PRANGE M. The effect of mountain uplift on eastern boundary currents and upwelling systems. *Climate of the Past*, 2020, 16(1): 161–181. https://doi.org/10.5194/cp-16-161-2020
[30] SILVA M., ARAUJO M., GEBER F., MEDEIROS C., ARAUJO J., NORIEGA C., and DA SILVA A. C. Ocean Dynamics and Topographic Upwelling Around the Aracati Seamount - North Brazilian Chain From in situ Observations and Modeling Results. *Frontiers in Marine Science*, 2021, 8: 609113. https://doi.org/10.3389/fmars.2021.609113
[31] XIE S., HUANG Z, and WANG X. H. Remotely Sensed Seasonal Shoreward Intrusion of the East Australian Current: Implications for Coastal Ocean Dynamics. *Remote Sensing*, 2021, 13(5): 854. https://doi.org/10.3390/rs13050854
[32] RUSSO C. S., LAMONT T., TUTT G. C. O., VAN DEN BERG M. A., and BARLOW R. G. Hydrography of a shelf ecosystem inshore of a major Western Boundary Current. *Estuarine, Coastal and Shelf Science*, 2019, 228: 106363. https://doi.org/10.1016/j.ecss.2019.106363
[33] LIAO F., LIANG X., LI Y., and THURNHERR A. Intense Subsurface Upwelling Associated with Major Western Boundary Currents. Proceedings of the 22nd EGU General Assembly, 2020. https://doi.org/10.5194/egusphere-egu2020-6214
[34] TROWBRIDGE J. H., & LENTZ S. J. The bottom boundary layer. *Annual Review of Marine Science*, 2018, 10: 397–420. https://doi.org/10.1146/annurev-marine-121916-063351
[35] KUNARSO, HADI S., SARI NINGSIH N., BASKORO M. S., WIRASATRIYA A., and KUSWARDANI A. R. T. D. The classification of upwelling indicators base on sea surface temperature, chlorophyll-a and upwelling index, the case study in Southern Java to Timor Waters. *IOP Conference Series: Earth and Environmental Science*, 2020, 530: 12020. https://doi.org/10.1088/1755-1315/530/1/012020
[36] WIRASATRIYA A., SUSANTO R. D., KUNARSO K., JALIL A. R., RAMDANI F., and PURYAJATI A. D. Northwest monsoon upwelling within the Indonesian seas. *International Journal of Remote Sensing*, 2021, 42(14): 5437–5458. https://doi.org/10.1080/01431161.2021.1918790
[37] BRINK K. H. Rectified flow in a stratified coastal ocean. *Journal of Marine Research*, 2018, 76(1): 1–22. https://doi.org/10.1357/002224018824082016
[38] RIBBE J., TOASPERN L., WOLFF J.-O., and ISMAIL M. F. A. Frontal eddies along a western boundary current. *Continental Shelf Research*, 2018, 165: 51–59. https://doi.org/10.1016/j.csr.2018.06.007
[39] HORII T., UEKI I., and ANDO K. Coastal upwelling events along the southern coast of Java during the 2008 positive Indian Ocean Dipole. *Journal of Oceanography*, 2018, 74(5): 499-508. https://doi.org/10.1007/s10872-018-0475-z
[40] NAULITA Y., ARHATIN R. E., and NABIL. Upwelling index along the South Coast of Java from satellite imagery of wind stress and sea surface temperature. *IOP Conference Series: Earth and Environmental Science*, 2020, 429: 012025. https://doi.org/10.1088/1755-1315/429/1/012025
[41] FADLAN A., SUGIANTO D. N., KUNARSO, and ZAINURI M. Influence of ENSO and IOD to Variability of Sea Surface Height in the North and South of Java Island. *IOP Conference Series: Earth and Environmental Science*, 2017, 55: 12021. https://doi.org/10.1088/1742-6596/755/1/011001
[42] ZHENG G., & DI GIACOMO P. M. Remote sensing of chlorophyll-a in coastal waters based on the light absorption coefficient of phytoplankton. *Remote Sensing of Environment*, 2017, 201: 331–341. https://doi.org/10.1016/j.rse.2017.09.008
[43] ISMAIL M. F. A., RIBBE J., and KARSTENSEN J. Remote sensing of upwelling off Australia's north-east coast. *Ocean Science Discussions*, 2019. https://doi.org/10.5194/os-2018-14
[44] FERNANDEZ E., & LELLOUCHE J. M. *Product User Manual for the Global Ocean Physical Reanalysis Product. GLOBAL_REANALYSIS_PHY_001_030*. 2018. https://resources.marine.copernicus.eu/documents/PUM/CMEMS-GLO-PUM-001-030.pdf
[45] BERMUDEZ. *On the Empirical Orthogonal Functions Representation of the Ocean*. Doctoral thesis. Universität Hamburg, Hamburg, 2020.
[46] THOMSON R. E., & EMERY W. J. *Data Analysis Methods in Physical Oceanography.* 3rd ed. Elsevier, Waltham, Massachusetts, 2014. https://www.elsevier.com/books/data-analysis-methods-in-physical-oceanography/thomson/978-0-12-387782-6

[47] CORREDOR-ACOSTA A., PIZARRO-KOCH M., MEDELL J., and SALD G. S. Spatio-Temporal Variability of Chlorophyll-A and Environmental Variables in the Panama Bight. *Remote Sensing*, 2020, 12(13): 2150. https://doi.org/10.3390/rs12132150
[48] CAVANAUGH J. E., & NEATH A. A. The Akaike information criterion: Background, derivation, properties, application, interpretation, and refinements. *Wiley Interdisciplinary Reviews: Computational Statistics*, 2019, 11(3): e1460. https://doi.org/10.1002/wics.1460
[49] SATHYENDRANATH S., BREWIN R. J. W., BROCKMANN C., BROTAS V., CALTON B., CHUPRIN A., CIPOLLINI P., COUTO A. B., DINGLE J., DOERFFER R., DONLON C., DOWELL M., FARMAN A., GRANT M., GROOM S., HORSEMAN A., JACKSON T., KRASEMANN H., LAVENDER S., MARTINEZ-VICENTE V., MAZERAN C., MÉLIN F., MOORE T. S., MÜLLER D., REGNER P., ROY S., STEELE C. J., STEINMETZ F., SWINTON J., TABERNER M., THOMPSON A., VALENTE A., ZÜHLKE M., BRANDO V. E., FENG H., FELDMAN G., FRANZ B. A., FROUIN R., GOULD R. W., HOOKER S. B., KAHRU M., KRATZER S., MITCHELL B. G., MULLER-KARGER F. E., SOSIK H. M., VOSS K. J., WERDELL J., and PLATT T. An ocean-colour time series for use in climate studies: The experience of the ocean-colour climate change initiative (OC-CCI). *Sensors*, 2019, 19(19): 4285. https://doi.org/10.3390/s19194285
[50] RIVAS M. B., & STOFFELEN A. Characterizing ERA-Interim and ERA5 surface wind biases using ASCAT. *Ocean Science*, 2019, 15(3): 831–852. https://doi.org/10.5194/os-15-831-2019
[51] HERSBACH H., BELL B., BERRISFORD P., HIRAHARA S., HORÁNYI A., MUÑOZ-SABATER J., NICOLAS J., PEUBEY C., RADU R., SCHEPERS D., SIMMONS A., SOCI C., ABDALLA S., ABELLAN X., BALSAMO G., BECHTOLD P., BIAVATI G., BIDLOT J., BONAVITA M., DE CHIARA G., DAHLGREN P., DEE D., DIAMANTAKIS M., DRAGANI R., FLEMMING J., FORBES R., FUENTES M., GEER A., HAIMBERGER L., HEALY S., HOGAN R. J., HÓLM E., JANISKOVÁ M., KEELEY S., LALOYAUX P., LOPEZ P., LUPU C., RADNOTI G., DE ROSNAY P., ROZUM I., VAMBORG F., VILLAUME S., and THÉPAUT J.-N. The ERA5 global reanalysis. *Quarterly Journal of the Royal Meteorological Society*, 2020, 146(730): 1999–2049. https://doi.org/10.1002/qj.3803
[52] HOFFMANN L., GÜNTHER G., LI D., STEIN O., WU X., GRIESSBACH S., HENG Y., KONOPKA P., MÜLLER R., VOGEL B., and WRIGHT J. S. From ERA-Interim to ERA5: The considerable impact of ECMWF's next-generation reanalysis on Lagrangian transport simulations. *Atmospheric Chemistry and Physics*, 2019, 19(5): 3097–3214. https://doi.org/10.5194/acp-19-3097-2019
[53] TAREK M., BRISSETTE F. P., and ARSENAULT R. Evaluation of the ERA5 reanalysis as a potential reference dataset for hydrological modelling over North America. *Hydrology and Earth System Sciences*, 2020, 24(5): 2527–2544. https://doi.org/10.5194/hess-24-2527-2020
[54] BRUNO M. F., MOLFETTA M. G., TOTARO V., and MOSSA M. Performance assessment of ERA5 wave data in a swell dominated region. *Journal of Marine Science and Engineering*, 2020, 8(3): 214. https://doi.org/10.3390/jmse8030214
[55] DRÉVILLON M., LELLOUCHE J.-M., RÉGNIER C., GARRIC G., BRICAUD C., HERNANDEZ O., and BOURDALLÉ-BADIE R. *Quality Information Document for Global Ocean Reanalysis Products. GLOBAL_REANALYSIS_PHY_001_030*. 2021. https://resources.marine.copernicus.eu/documents/QUID/CMEMS-GLO-QUID-001-030.pdf
[56] PURBA N. P., & KHAN A. M. A. Upwelling Session in Indonesia Waters. *World News of Natural Sciences*, 2019, 25: 72–83. http://yadda.icm.edu.pl/yadda/element/bwmeta1.element.psjd-f8f72649-9faa-478a-892e-b0da200dd60c
[57] BAYHAQI A., LENN Y. D., SURINATI D., POLTON J., NUR M., CORVIANAWATIE C., and PURWANDANA A. The variability of indonesian throughflow in Sumba Strait and its linkage to the climate events. *American Journal of Applied Sciences*, 2019, 16(4): 118-133. https://doi.org/10.3844/ajassp.2019.118.133
[58] ALVES J. M. R., PELIZ A., CALDEIRA R. M. A., and MIRANDA P. M. A. Atmosphere-ocean feedbacks in a coastal upwelling system. *Ocean Modelling*, 2018, 123: 55–65. https://doi.org/10.1016/j.ocemod.2018.01.004
[59] PEI S., LAWS E. A., ZHU Y., ZHANG H., YE S., YUAN H., and DING X. Nutrient dynamics and their interaction with phytoplankton growth during autumn in Liaodong Bay, China. *Continental Shelf Research*, 2019, 186: 34–47. https://doi.org/10.1016/j.csr.2019.07.012
[60] PACZKOWSKA J., ROWE O. F., FIGUEROA D., and ANDERSSON A. Drivers of phytoplankton production and community structure in nutrient-poor estuaries receiving terrestrial organic inflow. *Marine Environmental Research*, 2019, 151: 104778. https://doi.org/10.1016/j.marenvres.2019.104778
[61] EUROPEAN CENTRE FOR MEDIUM-RANGE WEATHER FORECASTS. *ERA5 Reanalysis (0.25 Degree Latitude-Longitude Grid)*. Research Data Archive at the National Center for Atmospheric Research, Computational and Information Systems Laboratory, 2019. https://doi.org/10.5065/BH6N-5N20
[62] COPERNICUS. n.d. https://resources.marine.copernicus.eu/

参考文:

[1] ROSS T.、CRAIG S. E.、COMEAU A.、DAVIS R.、DEVER M. 和 BECK M. 苏格兰大陆架上的绽放和地下浮游植物层：分析滑翔机的见解。海洋系统杂志，2017，172：118-127。https://doi.org/10.1016/j.jmarsys.2017.03.007
[2] TWEDDLE J. F.、GUBBINS M. 和 SCOTT B. E. 浮游植物是否应该成为海洋管理的关键考虑因素？海洋政策，2018，97：1-9。https://doi.org/10.1016/j.marpol.2018.08.026
[3] ARMENGOL L.、CALBET A.、FRANCHY G.、RODRÍGUEZ-SANTOS A. 和 HERNÁNDEZ-LEÓN S. 热带和亚热带大西洋沿生产力梯度的浮游食物网结构和营

养转移效率。科学报告，2019，9：2044。https://doi.org/10.1038/s41598-019-38507-9
[4] SALGADO-HERNANZ P. M.、RACAULT M. F.、FONT-MUÑOZ J. S. 和 BASTERRETXEA G. 基于海洋颜色遥感的地中海浮游植物物候趋势。环境遥感，2019，221：50-64。https://doi.org/10.1016/j.rse.2018.10.036
[5] LIM Y. K.、BAEK S. H.、LEE M.、KIM Y. O.、CHOI K. H., 和 KIM J. H. 与韩国南部海域夏季物理和化学变量相关的浮游植物组成：两种有毒鞭毛藻甲藻 的演替意义（又名海参）多棱锥和亚历山大仿射。实验海洋生物学与生态学杂志，2019，516：51-66。https://doi.org/10.1016/j.jembe.2019.05.006
[6] CORREDOR-ACOSTA A.、MORALES C. E.、BREWIN R. J. W.、AUGER P.-A.、PIZARRO O.、HORMAZABAL S. 和 ANABALÓN V. 与智利中南部附近的中尺度涡流相关的浮游植物大小结构：卫星浮游植物大小级模型的应用。遥感，2018，10(6): 834. https://doi.org/10.3390/rs10060834
[7] RUIZ S.、CLARET M.、PASCUAL A.、OLITA A.、TROUPIN C.、CAPET A.、TOVAR-SÁNCHEZ A.、ALLEN J.、POULAIN P.-M.、TINTORÉ J. 和 MAHADEVAN A. 海洋中尺度和亚中尺度锋面过程对浮游植物垂直输送的影响。地球物理研究杂志：海洋，2019，124(8)：5999–6014。https://doi.org/10.1029/2019JC015034
[8] GEBREHIWOT M.、KIFLE D. 和 TRIEST L. 划分流体动力学引起的物理变量和营养物对浅层热带水库（科卡，埃塞俄比亚）中浮游植物组合的影响。湖沼学，2020, 21(3): 269–274。https://doi.org/10.1007/s10201-020-00611-5
[9] GAO C., FU M., SONG H., WANG L., WEI Q., SUN P., LIU L., 和 ZHANG X. 南爪哇沿海上升流系统中亚表层叶绿素最大值中的浮游植物色素模式，印度尼西亚。海洋学报，2018，37（12）：97-106。https://doi.org/10.1007/s13131-018-1342-x
[10] GROOM S. B.、SATHYENDRANATH S.、BAN Y.、BERNARD S.、BREWIN R.、BROTAS V.、BROCKMANN C.、CHAUHAN P.、CHOI J.-K.、CHUPRIN A.、CIAVATTA S.、CIPOLLINI P., DONLON C., FRANZ B., HE X., HIRATA T., JACKSON T., KAMPEL M., KRASEMANN H., LAVENDER S., PARDO-MARTINEZ S., MÉLIN F., PLATT T., SANTOLERI R.、SKAKALA J.、SCHAEFFER B.、SMITH M.、STEINMETZ F.、VALENTE A. 和 WANG M. 卫星海洋颜色：现状和未来展望。海洋科学前沿，2019，6：485。https://doi.org/10.3389/fmars.2019.00485
[11] HOOD R. R.、BECKLEY L. E. 和 WIGGERT J. D. 印度洋边界流的生物地球化学和生态影响。海洋学进展，2017，156：290-325。https://doi.org/10.1016/j.pocean.2017.04.011
[12] LAHLALI H.、WIRASATRIYA A.、GENSAC E.、HELMI M.、KUNARSO 和 KISMAWARDHANI R. A. 基于卫星测量的爪哇南部海岸印度洋金枪鱼捕捞的环境方面。第四届地理信息学国际研讨会论文集，玛琅，2018，第 1-6 页。https://doi.org/10.1109/ISYG.2018.8612020
[13] DEWI A. K.、GAOL J. L.、SIREGAR V. P. 和 ATMADIPOERA A. S. 大眼睛金枪鱼渔场分析使用南爪哇东印度洋的海洋学特征。眼压会议系列：地球与环境科学，2020，429：012043。https://doi.org/10.1088/1755-1315/429/1/012043
[14] DUAN Y., LIU H., YU W., LIU L., YANG G., 和 LIU B. 由第一支向东传播的马登-朱利安振荡引发的印度尼西亚-澳大利亚夏季风的爆发。气候杂志，2019，32(17)：5453–5470。https://doi.org/10.1175/JCLI-D-18-0513.1
[15] RUDIASTUTI A. W.、SYAFI'I A. N. 和 KUSUMA H. A. 使用高度测量数据的印度尼西亚潮汐空间格局。第六届拉潘-知识产权局卫星国际研讨会论文集，茂物，2019。https://doi.org/10.1117/12.2542855
[16] KIM H.、VITART F. 和 WALISER D. E. 马登-朱利安振荡的预测：综述。气候杂志，2018, 31(23): 9425–9443。https://doi.org/10.1175/JCLI-D-18-0210.1
[17] 张 C., ADAMES F., KHOUIDER B., WANG B., 和 YANG D. 马登-朱利安振荡的四种理论。地球物理学评论，2020，58(3)：e2019RG000685。https://doi.org/10.1029/2019RG000685
[18] MENEZES V. V., & VIANNA M. L. 南印度洋准两年一次的罗斯比和开尔文波：热带和亚热带模式和印度洋偶极子。深海研究第二部分：海洋学专题研究，2019，166：43-63。https://doi.org/10.1016/j.dsr2.2019.05.002
[19] PUJIANA K., & MCPHADEN M. J. 赤道印度洋的季内开尔文波及其向印度尼西亚海的传播。地球物理研究杂志：海洋，2020，125（5）：1-25。https://doi.org/10.1029/2019JC015839
[20] HAMEED S. N. 印度洋偶极子。牛津研究百科全书：气候科学，2018，1：1-35。https://doi.org/10.1093/acrefore/9780190228620.013.619

[21] WIRASATRIYA A.、KUNARSO K.、MASLUKAH L.、SATRIADI A. 和 ARMANTO R. D. 叶绿素 a 浓度和海面温度 (不锈钢) 对巽他海峡东南风的不同响应。眼压会议系列：地球与环境科学，2018，139：012028。https://doi.org/10.1088/1755-1315/139/1/012028
[22] NINGSIH N. S.、SAKINA S. L.、SUSANTO R. D. 和 HANIFAH F. 东南热带印度洋 (设置) 的带状流特征。海洋科学讨论，2020。https://doi.org/10.5194/os-2020-91
[23] PANG X.、BASSINOT F. 和 SEPULCRE S. 过去两个冰期-间冰期循环中的印度尼西亚通流变化：来自东印度洋的证据。第四纪科学评论，2021，256：106839。https://doi.org/10.1016/j.quascirev.2021.106839
[24] UTARI P. A.、SETIABUDIDAYA D.、KHAKIM M. Y. N. 和 ISKANDAR I. 拉马观测网络揭示的南爪哇海岸流动力学。陆地、大气和海洋科学，2019，30(2)：235–245。 https://doi.org/10.3319/TAO.2018.12.14.01
[25] YANG G., ZHAO X., LI Y., LIU L., WANG F., 和 YU W. 热带印度洋东南部中尺度涡旋引起的叶绿素变异。海洋系统杂志，2018，199：103209。https://doi.org/10.1016/j.jmarsys.2019.103209
[26] ISMAIL M. F. A.、RIBBE J.、ARIFIN T.、TAOFIQUROHMAN A. 和 ANGGORO D. 印度洋热带东部边界涡旋普查。地球物理研究杂志：海洋，2021，126(6)：e2021JC017204。https://doi.org/10.1029/2021JC017204
[27] WIRASATRIYA A.、SETIAWAN J. D.、SUGIANTO D. N.、ROSYADI I. A.、HARYADI H.、WINARSO G.、SETIAWAN R. Y. 和 SUSANTO R. D. 埃克曼沿爪哇南部海岸的动态变化由卫星数据揭示。国际遥感杂志，2020，41(21)：8475–8496。https://doi.org/10.1080/01431161.2020.1797215
[28] DAI S., ZHAO Y., LI X., WANG Z., ZHU M., LIANG J., LIU H., TIAN Z., 和 SUN X. 热带西太平洋海山对浮游植物的影响。海洋环境研究，2020，162：105094。https://doi.org/10.1016/j.marenvres.2020.105094
[29] JUNG G., & PRANGE M. 山脉隆起对东部边界流和上升流系统的影响。过去的气候，2020，16（1）：161-181。 https://doi.org/10.5194/cp-16-161-2020
[30] SILVA M.、ARAUJO M.、GEBER F.、MEDEIROS C.、ARAUJO J.、NORIEGA C. 和 DA SILVA A. C. 阿拉卡蒂海山周围的海洋动力学和地形上升流 - 来自原位观测和建模的巴西北部链结果。海洋科学前沿，2021，8：609113。https://doi.org/10.3389/fmars.2021.609113
[31] XIE S., HUANG Z, 和 WANG X. H. 遥感季节性海岸入侵东澳大利亚洋流：对沿海海洋动力学的影响。遥感，2021, 13(5): 854. https://doi.org/10.3390/rs13050854
[32] RUSSO C. S.、LAMONT T.、TUTT G. C. O.、VAN DEN BERG M. A. 和 BARLOW R. G. 主要西部边界流近岸陆架生态系统的水文学。河口，沿海和陆架科学，2019，228：106363。https://doi.org/10.1016/j.ecss.2019.106363
[33] LIAO F., LIANG X., LI Y., 和 THURNHERR A. 与主要西部边界流相关的强烈地下上升流。 2020 年第 22 届 EGU 大会会议记录。https://doi.org/10.5194/egusphere-egu2020-6214
[34] TROWBRIDGE J. H., & LENTZ S. J. 底部边界层。海洋科学年度评论，2018，10：397-420。https://doi.org/10.1146/annurev-marine-121916-063351
[35] KUNARSO, HADI S., SARI NINGSIH N., BASKORO MS, WIRASATRIYA A., 和 KUSWARDANI A. R. T. D. 基于海面温度、叶绿素 a 和上升流指数的上升流指标分类，南爪哇到帝汶的案例研究沃特斯。眼压会议系列：地球与环境科学，2020，530：12020。https://doi.org/10.1088/1755-1315/530/1/012020
[36] WIRASATRIYA A.、SUSANTO R. D.、KUNARSO K.、JALIL A. R.、RAMDANI F. 和 PURYAJATI A. D. 印度尼西亚海域内上升流的西北季风。国际遥感杂志，2021，42(14)：5437–5458。https://doi.org/10.1080/01431161.2021.1918790
[37] BRINK K. H. 分层沿海海洋中的整流流。海洋研究杂志，2018，76（1）：1-22。https://doi.org/10.1357/002224018824082016
[38] RIBBE J.、TOASPERN L.、WOLFF J.-O. 和 ISMAIL M. F. A. 沿西部边界流的锋面涡流。大陆架研究，2018，165：51-59。 https://doi.org/10.1016/j.csr.2018.06.007
[39] HORII T.、UEKI I. 和 ANDO K. 2008 年正印度洋偶极子期间爪哇南部海岸的沿海上升流事件。海洋学杂志，2018, 74(5): 499-508。https://doi.org/10.1007/s10872-018-0475-z
[40] NAULITA Y.、ARHATIN R. E. 和 NABIL。来自风应力和海面温度卫星图像的爪哇南海岸上升流指数。眼压会议系列：地球与环境科学，2020，429：012025。https://doi.org/10.1088/1755-1315/429/1/012025
[41] FADLAN A.、SUGIANTO D. N.、KUNARSO 和 ZAINURI M. ENSO 和 IOD 对爪哇岛北部和南部海面高度变化的影响。眼压会议系列：地球与环境科学，2017，55：12021。 https://doi.org/10.1088/1742-6596/755/1/011001

[42] ZHENG G., & DI GIACOMO P. M. 基于浮游植物光吸收系数的沿海水域叶绿素-a 遥感。环境遥感，2017，201：331-341。 https://doi.org/10.1016/j.rse.2017.09.008

[43] ISMAIL M. F. A.、RIBBE J. 和 KARSTENSEN J. 澳大利亚东北海岸上升流的遥感。海洋科学讨论，2019。https://doi.org/10.5194/os-2018-14

[44] FERNANDEZ E., & LELLOUCHE J. M. 全球海洋物理再分析产品用户手册。GLOBAL_REANALYSIS_PHY_001_030 。 2018. https://resources.marine.copernicus.eu/documents/PUM/CMEMS-GLO-PUM-001-030.pdf

[45] 贝穆德斯。关于海洋的经验正交函数表示。博士论文。汉堡大学，汉堡，2020。

[46] THOMSON R. E., & EMERY W. J. 物理海洋学中的数据分析方法。第 3 版。爱思唯尔，马萨诸塞州沃尔瑟姆， 2014 。 https://www.elsevier.com/books/data-analysis-methods-in-physical-oceanography/thomson/978-0-12-387782-6

[47] CORREDOR-ACOSTA A.、PIZARRO-KOCH M.、MEDELL J. 和 SALD G. S. 巴拿马湾中叶绿素—种和环境变量的时空变异性。遥感，2020，12(13)：2150. https://doi.org/10.3390/rs12132150

[48] CAVANAUGH J. E., & NEATH A. A. 赤池信息准则：背景、推导、性质、应用、解释和改进。威利跨学科评论：计算统计， 2019， 11(3) ： e1460 。 https://doi.org/10.1002/wics.1460

[49] SATHYENDRANATH S., BREWIN R. J. W., BROCKMANN C., BROTAS V., CALTON B., CHUPRIN A., CIPOLLINI P., COUTO A. B., DINGLE J., DOERFFER R., DONLON C., DOWELL M., FARMAN A., GRANT M., GROOM S., HORSEMAN A., JACKSON T., KRASEMANN H., LAVENDER S., MARTINEZ-VICENTE V., MAZERAN C., MÉLIN F., MOORE T. S., MÜLLER D., REGNER P., ROY S., STEELE C. J., STEINMETZ F., SWINTON J., TABERNER M., THOMPSON A., VALENTE A., ZÜHLKE M., BRANDO V. E., FENG H., FELDMAN G., FRANZ B. A., FROUIN R., GOULD R. W., HOOKER S. B., KAHRU M., KRATZER S., MITCHELL B. G., MULLER-KARGER F. E., SOSIK H. M., VOSS K. J., WERDELL J., 和 PLATT T. 用于气候研究的海洋色时间序列：这海洋颜色气候变化倡议 (超频-CCI) 的经验。传感器，2019，19(19)：4285. https://doi.org/10.3390/s19194285

[50] RIVAS M. B., & STOFFELEN A. 使用 ASCAT 表征时代-临时和时代 5 表面风偏。海洋科学，2019，15(3)：831–852。 https://doi.org/10.5194/os-15-831-2019

[51] HERSBACH H., BELL B., BERRISFORD P., HIRAHARA S., HORÁNYI A., MUÑOZ-SABATER J., NICOLAS J., PEUBEY C., RADU R., SCHEPERS D., SIMMONS A., SOCI C., ABDALLA S., ABELLLAN X., BALSAMO G., BECHTOLD P., BIAVATI G., BIDLOT J., BONAVITA M., DE CHIARA G., DAHLGREN P., DEE D., DIAMANTAKIS M., DRAGANI R., FLEMMING J., FORBES R., FUENTES M., GEER A., HAIMBERGER L., HEALY S., HOGAN R. J., HÓLM E., JANISKOVÁ M., KEELEY S., LALOYAUX P., LOPEZ P., LUPU C.、RADNOTI G. 、 DE ROSNAY P. 、 ROZUM I. 、VAMBORG F.、VILLAUME S. 和 THÉPAUT J.-N. 时代 5 全球再分析。皇家气象学会季刊，2020，146(730)：1999-2049。 https://doi.org/10.1002/qj.3803

[52] HOFFMANN L.、GÜNTHER G.、LI D.、STEIN O.、WU X.、GRIESSBACH S.、HENG Y.、KONOPKA P.、MÜLLER R.、VOGEL B. 和 WRIGHT J. S. 来自时代-临时时代 5：ECMWF 下一代再分析对拉格朗日输运模拟的重大影响。大气化学与物理，2019，19(5)：3097–3214。 https://doi.org/10.5194/acp-19-3097-2019

[53] TAREK M.、BRISSETTE F. P. 和 ARSENAULT R. 评估时代 5 再分析作为北美水文建模的潜在参考数据集。水文与地球系统科学，2020，24(5)：2527–2544。 https://doi.org/10.5194/hess-24-2527-2020

[54] BRUNO M. F.、MOLFETTA M. G.、TOTARO V. 和 MOSSA M. 时代 5 波浪数据在涌浪主导区域的性能评估。海洋科学与工程杂志，2020，8(3)：214. https://doi.org/10.3390/jmse8030214

[55] DRÉVILLON M.、LELLOUCHE J.-M.、RÉGNIER C.、GARRIC G.、BRICAUD C.、HERNANDEZ O. 和 BOURDALLÉ-BADIE R. 全球海洋再分析产品的质量信息文件。GLOBAL_REANALYSIS_PHY_001_030。2021. https://resources.marine.copernicus.eu/documents/QUID/CMEMS-GLO-QUID-001-030.pdf

[56] PURBA N. P., & KHAN A. M. A. 印度尼西亚水域的上升流会议。世界自然科学新闻，2019，25：72-83。 http://yadda.icm.edu.pl/yadda/element/bwmeta1.element.psjd-f8f72649-9faa-478a-892e-b0da200dd60c

[57] BAYHAQI A.、LENN Y. D.、SURINATI D.、POLTON J.、NUR M.、CORVIANAWATIE C. 和 PURWANDANA A. 松巴海峡印度尼西亚通流的变化及其与气候事件的联系。美国应用科学杂志，2019，16(4)：118-133。 https://doi.org/10.3844/ajassp.2019.118.133

[58] ALVES J. M. R.、PELIZ A.、CALDEIRA R. M. A. 和 MIRANDA P. M. A. 沿海上升流系统中的大气-海洋反馈。海洋建模， 2018 ， 123 ： 55-65 。 https://doi.org/10.1016/j.ocemod.2018.01.004

[59] PEI S.、LAWS E. A.、ZHU Y.、ZHANG H.、YE S.、YUAN H. 和 DING X. 中国辽东湾秋季营养动态及其

与浮游植物生长的相互作用。大陆架研究，2019，186：34-47。 https://doi.org/10.1016/j.csr.2019.07.012
[60] PACZKOWSKA J.、ROWE O. F.、FIGUEROA D. 和 ANDERSSON A. 接受陆地有机流入的营养贫乏河口中浮游植物生产和群落结构的驱动因素。海洋环境研究，2019，151：104778。 https://doi.org/10.1016/j.marenvres.2019.104778
[61] 欧洲中程天气预报中心. 时代 5 再分析（0.25 度经纬度网格）。国家大气研究中心、计算和信息系统实验室的研究数据档案，2019。 https://doi.org/10.5065/BH6N-5N20
[62] 哥白尼。日期 https://resources.marine.copernicus.eu/